SLENDER FISH LIFT AND MOMENT

by

William M. Simpson, Jr.

SLENDER FISH LIFT AND MOMENT

by

William Maurice Simpson, Jr., Lieutenant, United States Coast Guard

B. S., United States Coast Guard Academy
(1965)

SUBMITTED IN PARTIAL FULFILLMENT

OF THE REQUIREMENTS FOR THE

MASTER OF SCIENCE DEGREE IN NAVAL ARCHITECTURE AND MARINE ENGINEERING

AND THE PROFESSIONAL DEGREE, NAVAL ENGINEER

at the

MASSACHUSETTS INSTITUTE OF

TECHNOLOGY

JUNE, 1971

SLENDER FISH LIFT AND MOMENT

by

William Maurice Simpson, Jr., Lieutenant, United States Coast Guard

Submitted to the Department of Naval Architecture and Marine Engineering in partial fulfillment of the requirements for the degree of Master of Science in Naval Architecture and Marine Engineering and the professional degree, Naval Engineer.

ABSTRACT

The lift and longitudinal moment are experimentally measured for a three-member family of flat plate fish forms to determine the range of linearity as a function of angle of attack, and to determine the effect of the body on the tail-produced lift.

The basic fish form is circular arc generated with an overall length of 16.25 inches, a body width of four inches, and tail width of three inches. The three forms consist of a full fish, a fish body, and a fish head. The experimental data are presented from tests performed in the M. I. T. Marine Hydrodynamics Laboratory.

Two possible mathematical models are postulated and compared to the experimental results.

It is concluded that the lift and moment are highly non-linear functions of the angle of attack and that the body has a marked effect on the lift produced by the tail.

Thesis Supervisor: John N. Newman, Sc. D.
Title: Professor of Naval Architecture

Table of Contents

List of Figures

CHAPTER I - INTRODUCTION

The swimming of slender fish has been of academic interest since Lighthill's article (2)* was published in 1960. In that article he approached the swimming of fish by the use of unsteady slender body theory. He followed this up with articles in 1969 (3) and 1970 (4) which were refinements and improvements of the first article.

This topic was also the subject of papers by Professor Wu in 1970 (7) and 1971 (8) and of a letter by Professor Newman (5) in 1971. These investigations used Prandtl's acceleration potential to determine the cross-flow and thus the flow about the fish.

Both types of theory used slender body theory and the associated assumptions. Three questions which seem to arise in this type of development are:

(1) Is slender body theory applicable to a fish-shaped body?

(2) What is the linear range for lift as a function of angle of attack?

(3) What is the effect of the presence of a lifting surface ahead of the tail?

It is the purpose of this investigation to answer these three questions for a particular flat plate fish shape in steady flow at an angle of attack. This will not give the answers needed for the unsteady flow associated with the swimming of fish, but it will give an indication of what the theory should be for the limiting case of steady flow.

*Numbers in parentheses refer to references listed in the bibliography.

CHAPTER II - THEORY

The fish is first approached by means of slender body theory as was done by Lighthill in 1960 (2). Slender body theory gives the lift as:

$$l(x) = -\rho U \frac{d}{dx}\left(W m_a(x)\right)$$

$l(x)$ = local lift per length

ρ = fluid density

U = free stream fluid velocity

W = cross-flow velocity

$m_a(x)$ = local 2-D added mass for cross-flow plane

The right hand side of the above expression is the local change in the Z-directed momentum, the coordinate system being defined in Figure 1.

Within linear theory: $W = -U\alpha$

α = angle of attack

Defining the fish shape: $y = \pm h(x)$

Modeling the fish as a flat plate:

$$m_a(x) = \pi h^2(x)$$

$$l(x) = -\rho U \frac{d}{dx}\left(-U\alpha \pi h^2(x)\right)$$

L = total lift

$$L = \int_{-l_{L.E.}}^{0} -\rho U \frac{d}{dx}\left(-U\alpha \pi h^2(x)\right)dx$$

The limits of the integral above are due to the fact that there is no contribution to lift aft of the maximum span according to slender body

FISH
COORDINATE SYSTEM

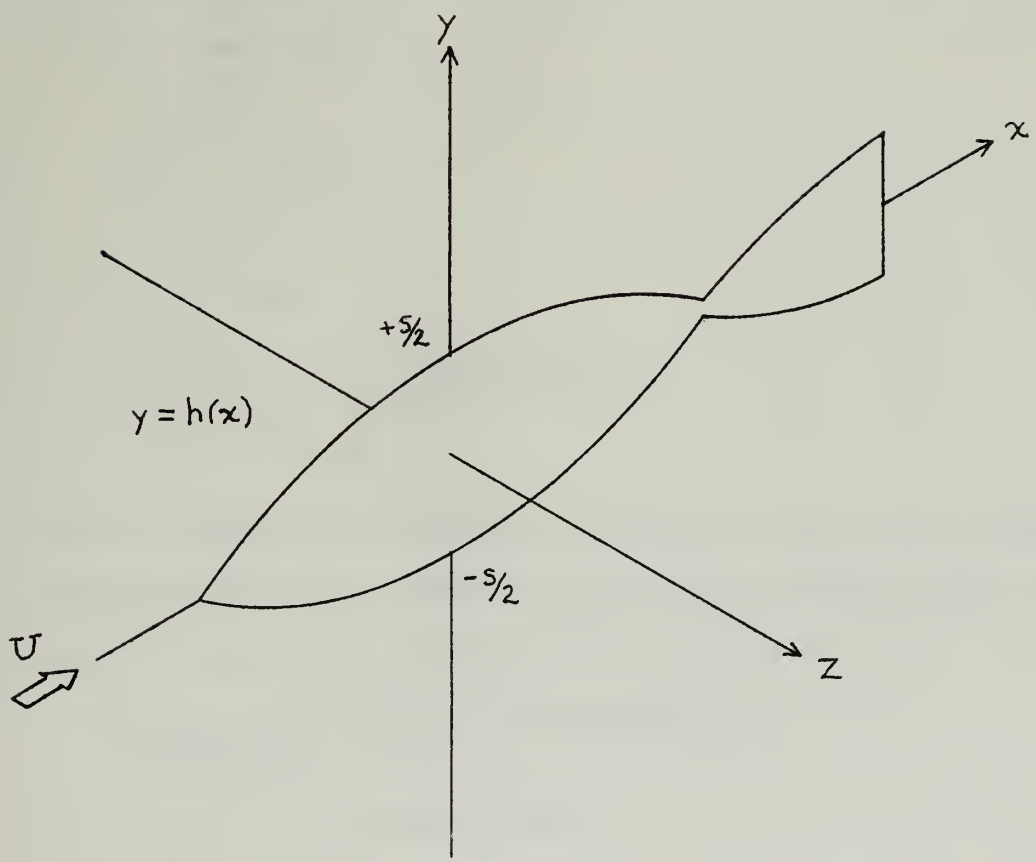

FIGURE 1

theory (note that the Z-directed momentum cannot be increased beyond that point).

$$L = +\rho U^2 \alpha \pi h^2(x) \Big|_{-l_{L.E.}}^{0}$$

since $h(-l_{L.E.}) = 0$

$$L = +\rho U^2 \alpha \pi h^2(0)$$

In a similar manner, moment is given by:

M ≡ moment about y axis

$$M = \int_{-l_{L.E.}}^{0} x l(x) dx$$

$$M = -\rho U \int_{-l_{L.E.}}^{0} x \frac{d}{dx} (-U\alpha \pi h^2(x)) \, dx$$

This lift predicted by slender body theory is known to be supplemented by a non-linear lift due to vorticity shed from the leading edges. This non-linear lift as cited in Thwaites (6) is suggested to be:

$$C_{L_{\text{non-linear}}} = (\tfrac{1}{2}\pi - \tfrac{1}{8}\pi \tan\varphi_L)\alpha^2$$

α = angle of attack

φ_L = angle of sweepback of leading edge

$$C_{L_{\text{non-linear}}} \equiv \frac{L_{\text{non-linear}}}{\frac{1}{2}\rho U^2 \text{ Area}}$$

This non-linear lift contribution has also been suggested by Lighthill (1) to be given by:

$$C_{L_{non\text{-}linear}} = C_{D_{cyl}} \alpha^2$$

$$L_{non\text{-}linear} = \tfrac{1}{2}\rho U^2 \text{ Area } C_{D_{cyl}} \alpha^2$$

$C_{D_{cyl}}$ = drag coefficient for cylinder of same cross-section

C_L and α are as defined above.

Looking at the non-linear lift on the head using the method of Thwaites (6) cited above, the non-linear lift is computed as follows:

$$\frac{L_{non\text{-}linear}}{\tfrac{1}{2}\rho U^2 \text{ Area}_h} = (\tfrac{1}{2}\pi - \frac{1}{8}\pi \tan \varphi_L)\alpha^2$$

Area_h = area of head = 16.35 in.

The head is modeled as a delta with a sweepback angle of 71.56 degrees.

$$\frac{L_{non\text{-}linear}}{\tfrac{1}{2}\rho U^2 \text{ Area}_h} = (\tfrac{1}{2}\pi - \frac{3}{8}\pi)\alpha^2$$

$$= \frac{\pi}{8}\alpha^2$$

Non-dimensionalizing, using the span squared vice the area for purposes of comparison with experimental data, the total C_L is given as:

$$C_{L_{head}} = \frac{L_{head}}{\tfrac{1}{2}\rho U^2 (2h(0))^2} = \frac{\pi}{2}\alpha + \frac{\pi}{8}\frac{\text{Area}_h}{(2h(0))^2}\alpha^2$$

$$C_{L_{head}} = 1.57\alpha + 0.402\alpha^2$$

For the fish body, this can be applied by replacing the area of the head by the area of the body.

$$C_{L_{body}} = 1.57\alpha + 0.803\alpha^2$$

If the full fish is modeled as a head followed by a rectangular plate of area equal to the area of the after body and the tail, the lift can be expressed as:

$$C_{L_{\text{full fish}}} = 1.57\alpha + 1.06\alpha^2$$

In order to better estimate the lift component produced by the tail of the fish, it is necessary to estimate the downwash at the tail produced by the vorticity shed by the body. In actuality, this vorticity will be in the form of a partially rolled up sheet. The slender body limit for small angles of attack suggests the lower limit of no lift on the tail. This model is contrasted with, first, a vortex sheet which follows the free stream back from the axis of maximum span, and then with a pair of fully rolled up vortices.

As a first estimate of downwash on the tail, a vortex sheet is placed in the x - y plane extending from y = -2 to y = +2 (see Figure 1). An elliptic spanwise vorticity distribution is used, as this will give a constant downwash at the section of maximum span and is consistant with the linear theory. For an elliptic distribution, we set:

$$\Gamma(y) = -2\,U\alpha a_1 \sqrt{1 - \left(\frac{2y}{s}\right)^2}$$

$\Gamma(y)$ = bound vorticity on fish head

a_1 = constant to be determined

The trailing vorticity, γ_x, is then given by:

$$\gamma_x = \frac{d}{dy}\Gamma(y)$$

$$\gamma_x(y) = +\frac{2U\alpha_1}{s}\,\frac{y}{\sqrt{1 - \left(\frac{2y}{s}\right)^2}}$$

Using an infinite vortex sheet and Biot-Savart's Law we have:

w = induced downwash velocity

$$w^* = \frac{1}{2\pi} \int_{-s/2}^{s/2} \frac{\gamma_x(\eta)\,(y-\eta)}{\left[(y-\eta)^2 + z^2\right]}\, d\eta$$

$$w^* = \frac{8Ua_1}{2\pi s} \int_{-s/2}^{s/2} \frac{\eta}{\sqrt{1-\left(\frac{2\eta}{s}\right)^2}} \frac{(y-\eta)\,d\eta}{\left[(y-\eta)^2 + z^2\right]}$$

Setting $y = 0$ to look at the centerline gives:

$$w^* = -\frac{8Ua_1}{2\pi s} \int_{-s/2}^{s/2} \frac{\eta^2\, d\eta}{\sqrt{1-\left(\frac{2\eta}{s}\right)^2}\,\left[\eta^2 + z^2\right]}$$

Setting $\eta = -s/2 \cos\varphi$ $\qquad$ $\eta = -s/2$ $\qquad$ $\varphi = 0$

$d\eta = s/2 \sin\varphi d\varphi$ $\qquad$ $\eta = +s/2$ $\qquad$ $\varphi = \pi$

$$w^* = -\frac{8Ua_1}{2\pi s} \frac{s}{2} \int_0^{\pi} \frac{\cos^2\varphi \sin\varphi\, d\varphi}{\sqrt{1-\cos^2\varphi}\,\left[\cos^2\varphi + \frac{z^2}{s^2}\right]}$$

$$w^* = -\frac{2Ua_1}{\pi} \int_0^{\pi} \left\{ \frac{\cos^2\varphi}{\left[\cos^2\varphi + \frac{z^2}{s^2}\right]} - 1 + 1 \right\} d\varphi$$

$$w^* = -\frac{2Ua_1}{\pi} \left[-\frac{4z^2}{s^2} \int_0^{\pi} \frac{d\varphi}{\left[\left(1 + \frac{4z^2}{s^2}\right)\cos^2\varphi + \frac{4z^2}{s^2}\sin^2\varphi\right]} + \pi \right]$$

$$w^* = -2Ua_1 \left[\frac{-2|z|}{\sqrt{\quad + \left(\frac{2z}{\quad}\right)^2}} + 1 \right]$$

Solving for a_1 by setting $w^* = -U\alpha$ at $z = 0$.

$$W^* = -2Ua_1 = -U\alpha$$

$$a_1 = \frac{\alpha}{2}$$

$$W^* = -U\alpha \left[1 - \frac{2|z|}{s\sqrt{1 + \left(\frac{2z}{s}\right)^2}}\right]$$

Looking at $z = \frac{7.6}{12} \sin \alpha$ as the lateral displacement of the center of the tail:

$$\frac{2z}{s} = 3.8 \sin \alpha$$

$$W^* = -U\alpha \left[1 \frac{-3.8 \sin \alpha}{\sqrt{1 + 14.43 \sin^2 \alpha}}\right]$$

This can be written as a series expansion for small angles as follows:

$$W^* \approx -U\alpha \left[1 - 3.8 \sin \alpha + 28.4 \sin^3 \alpha + 0 (\sin^5 \alpha)\right]$$

Using slender body theory following Newman (5) and Wu (7), and assuming that the effective velocity is equal to the velocity at the center for small angles, we can write:

$$L_{tail} = \rho \pi \left(\frac{s_T}{2}\right)^2 U (U\alpha + W^*)$$

where s_T = maximum width on the tail

$$L_{tail} = \rho \pi \left(\frac{s_T}{2}\right)^2 U^2 \alpha \left[3.8 \sin \alpha - 0 (\sin^3 \alpha)\right]$$

$$C_{L_{tail}} = 2 \left(\frac{s_T}{2s}\right)^2 \pi \alpha \left[3.8 \sin \alpha - 0 (\sin^3 \alpha)\right]$$

$$C_{L_{tail}} \approx 3.35 \alpha^2$$

Adding this to the earlier value of C_L we have:

$$C_{L_{full\ fish}} = 1.57\alpha + 4.41\alpha^2$$

This value of C_L has been obtained by assuming that the average downwash velocity is equal to the downwash on the centerline. This is valid for small angles; however, reference to Thwaites page 546 shows that for

this fish at angles of attack greater than ten degrees the average downwash is less than 75% of the downwash on the centerline. This in turn suggests that the α^2 term should have a somewhat larger coefficient. In spite of this consideration, it is felt that the expression for C_L given above does indicate correct trends for the vortex sheet model.

The downwash on the centerline due to two line vorticies trailing straight aft from the axis of maximum span is now considered as the second case. This is taken as a limit since it will place the vorticity the farthest from the centerline, giving the least downwash and therefore the most lift.

Placing line vorticies at $y = \pm 1.5$ inches and $z = 0$ and using Biot-Savart's Law and infinite line vorticies, the downwash is given by:

$$W^* = \frac{-(y + \frac{1.5}{12})\Gamma_x}{2\pi\left[(y + \frac{1.5}{12})^2 + z^2\right]} + \frac{(y - \frac{1.5}{12})\Gamma_y}{2\pi\left[(y - \frac{1.5}{12})^2 + z^2\right]}$$

W^* = downwash at (y,z) due to line vorticies at $y = \pm \frac{1.5}{12}$, $z = 0$.

Γ_x = strength of trailing vorticies

Setting $y = 0$ to look at the centerline and $z = \frac{7.6}{12} \sin\alpha$ where 7.6 = inches from axis of maximum span to center of tail, the downwash is given by:

$$W^* = \frac{-18\,\Gamma_x}{\pi\left[2.25 + 57.7 \sin^2\alpha\right]}$$

From Kelvin's Theorem the sum of trailing vorticity, $2\Gamma_x$, must be equal to the total bound vorticity on the foil, Γ.

$$2\Gamma_x = \Gamma = \int_{-s/2}^{s/2} \Gamma(y)\, dy$$

But also:

$$L = \rho U \int_{-s/2}^{s/2} \Gamma(y)\, dy = \rho U \Gamma$$

From the slender body theory developed above:

$$L = \rho U^2 \alpha \pi \left(s/2\right)^2$$

$$\rho U^2 \alpha \pi \left(s/2\right)^2 = \rho U \Gamma$$

$$\Gamma = U \alpha \pi \left(s/2\right)^2$$

$$\Gamma_x = \frac{U}{2} \alpha \pi \left(s/2\right)^2$$

$$W^* = \frac{-18 \frac{U}{2} \alpha \pi \left(\frac{2}{12}\right)^2}{\pi\left[2.25 + 57.7 \sin^2\alpha\right]}$$

$$W^* = \frac{-U\alpha}{4\left[2.25 + 57.7 \sin^2\alpha\right]}$$

Using slender body theory following Newman (5) and Wu (7), we can now write the lift on the tail as:

$$L_{tail} = \rho \pi \left(\frac{s_T}{2}\right)^2 U \left(U\alpha + W^*\right)$$

where s_T = maximum width of the tail

$$L_{tail} = \rho \pi \left(\frac{s_T}{2}\right)^2 U^2\alpha \left(1 - \frac{1}{4\left[2.25 + 57.7 \sin^2\alpha\right]}\right)$$

$$L_{tail} = \rho \pi \left(\frac{s_T}{2}\right)^2 U^2 \frac{\alpha}{4} \left(\frac{8 + 230.8 \sin^2\alpha}{2.25 + 57.7 \sin^2\alpha}\right)$$

$$L_{tail} = \rho \pi \left(\frac{s_T}{2}\right)^2 U^2\alpha \left(0.891 + 2.845 \sin^2\alpha + 0\left(\sin^4\alpha\right)\right)$$

This shows that at higher angles of attack where the vortex sheet is expected to be fully rolled up at the tail, the lift on the tail could be

as much as about 0.9 of what slender body theory would predict for the tail in undisturbed flow.

For the particular fish form in question, the tail maximum width is 3/4 of the maximum width of the body, so it would be expected that the tail could increase the predicted slender body lift by as much as about 1/2. C_L on the tail is then approximated as:

$$C_{L_{tail}} \approx .883\alpha\ (0.891 + 2.845 \sin^3\alpha)$$

$$C_{L_{tail}} \approx .79\alpha + 2.52\alpha^3$$

When this is added to the C_L determined above, C_L is given as

$$C_L = 2.36\alpha + 1.06\alpha^2$$

It is seen that this model increases the linear term more and the non-linear term less than the vortex sheet presented above. This would seem to provide a means of interpreting the experimental results to be considered subsequently.

To check the two line vortex model further, the inclination of vortex lines to free stream can be checked by looking at the velocities induced at $y = \pm 1.5$ and $z = 0$.

$$W^*(\pm 1.5, 0) = \frac{-(3)(12)\Gamma_x}{2\pi 9}$$

$$W^*(\pm 1.5, 0) = \frac{-2\Gamma_x}{\pi}$$

$$W^*(\pm 1.5, 0) = \frac{-U}{2}\ \frac{\alpha\pi 2}{\pi}\ \left(\frac{s}{2}\right)^2$$

$$W^*(\pm 1.5, 0) = -U\alpha\left(\frac{s}{2}\right)^2$$

$$\frac{W^*(\pm 1.5, 0)}{U} = \frac{-\alpha}{36}$$

Thus the inclination of the vortex lines to free stream is expected to be slight and, therefore, a higher order effect.

CHAPTER III - EXPERIMENTAL PROCEDURE

In order to find the lift and moment on a flat plate fish form, it was chosen to construct a metal fish from $\frac{1}{4}$ inch aluminum plate and test it in the water tunnel at M. I. T. Marine Hydrodynamics Laboratory. A fish form generated by circular arcs was chosen as this could be easily machined while still representing the general shape of a fish. The dimensions and shape are shown in Figure 2 and the structural design data are given in Appendix A. The leading edges of the fish body and tail were faired to approximately half round and the trailing edges were sharpened.

As illustrated in Figure 2 and Figure 16, a three-fish family was constructed as a full fish with body and tail, a fish body without a tail, and a fish head only. The tail was made narrower than the body to accentuate the wake effects. The forms were mounted on a 3/4 inch diameter shaft for mounting in the existing rudder force dynamometer. The fish end of the shaft was faired into the fish form by applying epoxy putty.

The force dynamometer is so built that it mounts directly into the test section of the propeller tunnel and was configured to measure normal lift, tangential drag, and chordwise moment. The dynamometer and its use are more fully discussed in Appendix B.

As described in Appendix A the test section of the water tunnel was equipped so that a dummy shaft could be placed symmetrically with respect to the mounting shaft. This allowed the fish to be tested with and without a dummy shaft so that the influence of the mounting shaft on lift and moment could be inferred.

The three fish forms were tested at speeds of approximately five, ten and 13 feet per second. At five feet per second the three forms were tested

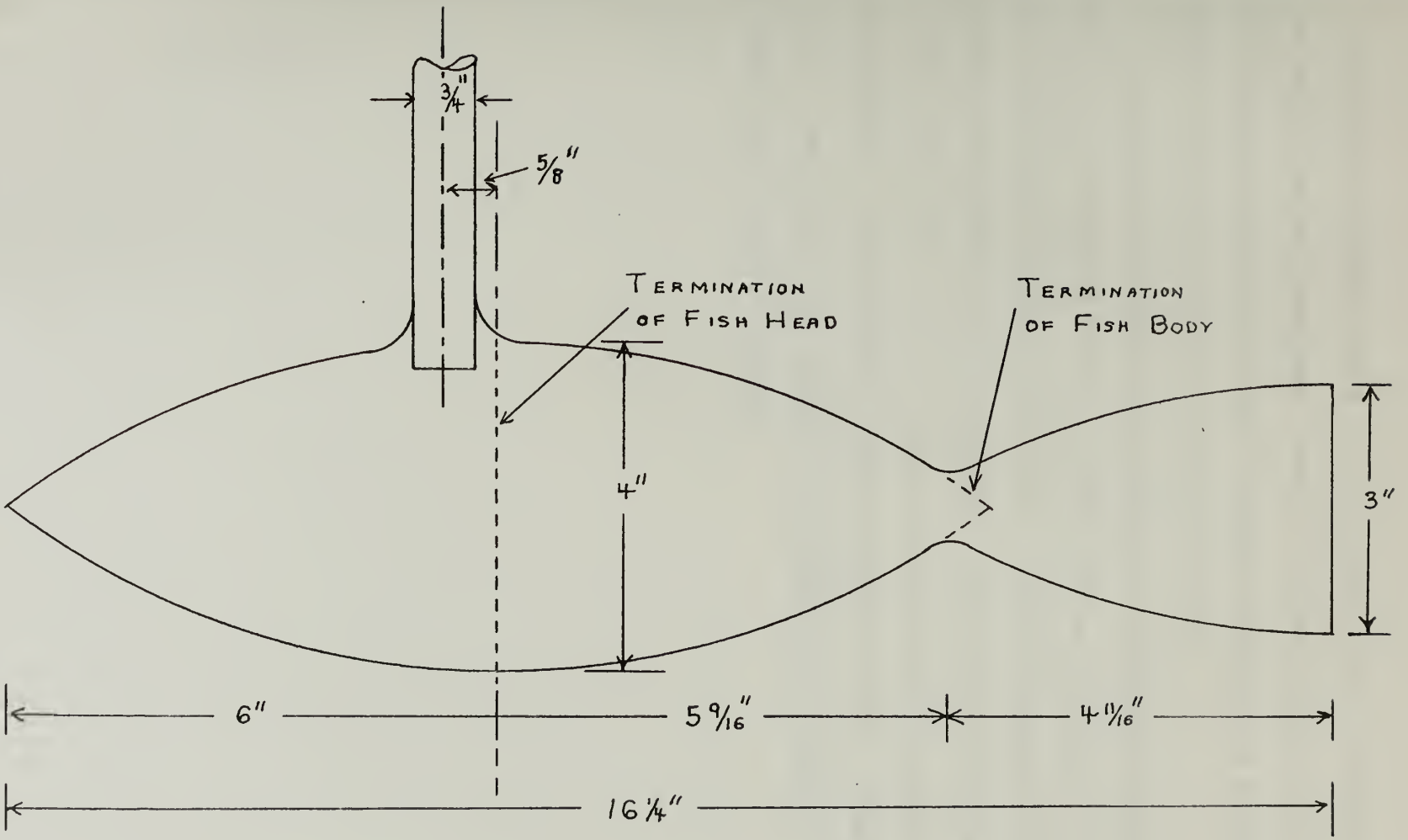

FISH FORMS

FIGURE 2

at two-degree intervals from 0 to -20 degrees, and at ten feet per second they were tested at two-degree intervals from +20 degrees to -20 degrees. The 13 feet per second tests used two-degree intervals up to only -12 degrees to keep the loading at acceptable levels.

As a means of indicating the shedding of vorticity, the full fish form was run at reduced tank pressure to produce cavitation. Pictures were taken using a Graphex camera with a Polaroid back and a Strobolume electronic stroboscopic flash using side lighting and a black back drop.

The outputs from the water tunnel manometer and the digital strain gauge readouts were fed into a computer program to yield streamwise lift, drag, and moment and flow velocity. The program also computed C_L and Lcp as described in the next section.

CHAPTER IV - EXPERIMENTAL RESULTS

The experimentally determined values of the lift and moment are shown in Figures 3 through 11. The lift and moment data have been converted to promote easy visualization and comparison between fish forms. The lift has been plotted as C_L which is defined as follows:

$$C_L = \frac{L}{\frac{1}{2}\rho U^2 (2h(0))^2}$$

where L = lift

ρ = fluid density

U = free stream velocity

$2h(0)$ = maximum span

The moment data are presented in the form of position of longitudinal center of pressure, Lcp, which is defined as follows:

$$Lcp = \frac{lcp}{6}$$

where lcp = distance of center of pressure forward of axis of maximum span

6 = distance from axis of maximum span to nose of the fish forms

As can be seen in Figures 3 through 11, the data points with and without the dummy strut have been plotted. The faired experimental line is plotted as an estimate of the extrapolation to no strut effects. The linear slender body theory values of C_L and Lcp have also been plotted for purposes of comparison.

Inspection of the Lcp data on Figures 3, 4, 7 and 10 shows a slight divergency below about five degrees. This divergence follows the division of + and - angles of attack which, together with the fact that the angles were always approached from the same side, would seem to indicate that this

divergence is due merely to a small instrument-generated moment which is only important at small values of lift and moment. It is felt that this effect was sufficiently straight forward that the overall results need not be questioned.

Figure 12 is a plot of the experimental data for the three fish forms for comparative purposes.

Looking back to the theory now we see that C_L is postulated as a function of α and α^2 for small angles. Thus C_L can be written as:

$$C_L = C_1\alpha + C_2\alpha^2$$

where C_1 and C_2 are constants to be determined.

In the development of the theory, it was assumed that:

$$U\alpha \approx U \sin\alpha$$

and

$$(U\alpha)^2 \approx U^2 \sin^2\alpha$$

Also note is taken of the fact that the α^2 term is assumed to represent a cross-flow drag which is normal to the surface rather than at right angles to the flow as the linear lift is assumed to be.

Thus C_L can be rewritten so as to be more accurate for large angles.

$$C_L = C_1 \sin\alpha + C_2 \sin^2\alpha \cos\alpha$$

Dividing by $\sin\alpha$:

$$\frac{C_L}{\sin\alpha} = C_1 + C_2 \sin\alpha \cos\alpha$$

$$\frac{C_L}{\sin\alpha} = C_1 + \frac{C_2}{2} \sin 2\alpha$$

Plotting $C_L/\sin\alpha$ versus $\sin 2\alpha$ and correcting for strut interference as above, we see that C_1 is given by the zero angle axis intercept and that

C_2 is given by twice the linear slope of the experimental data. Figures 13, 14 and 15 are plots of $C_L/\sin\alpha$ versus $\sin 2\alpha$ and show the associated values of C_1 and C_2 for the three fish forms.

Experimental error is seen in these plots in the form of scatter of the data points below five degrees. This is attributed to angle readings which were based on an experimental determination of angle of zero lift. Errors in this measurement show up at less than five degrees due to the fact that a small lift is being divided by a small angle function.

The three fish forms used in the force and moment measurements are shown in Figure 16.

The full fish form is shown in Figure 17 through 25 at various angles of attack at reduced pressure levels which cause the vortex cores to form cavities. This allows visualization of the line vorticies shed from the leading edge.

FULL FISH

VELOCITY 5 FPS

C_L AND L_{CP}

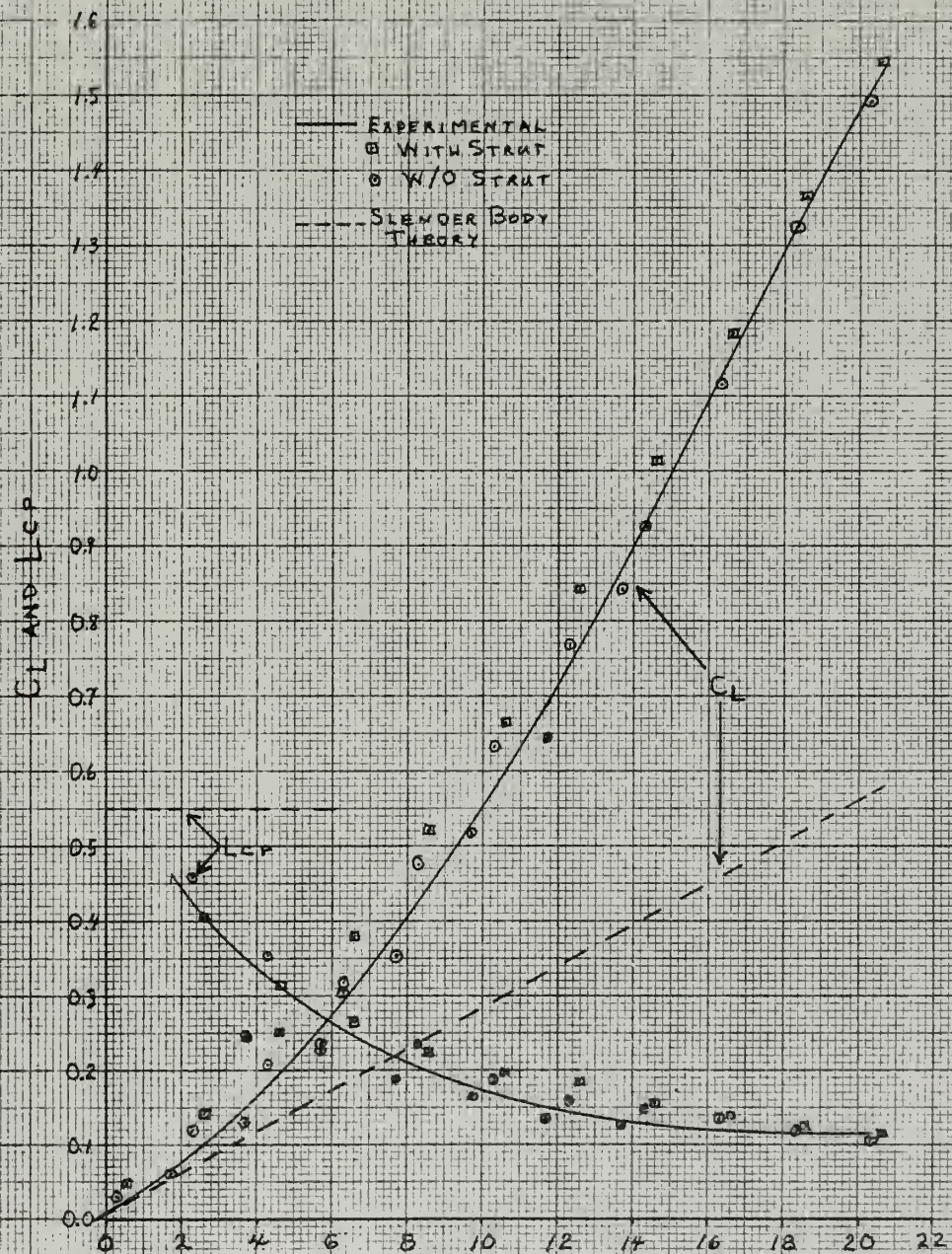

FIGURE 3

FULL FISH

VELOCITY 10 FPS

C_L AND L.C.P

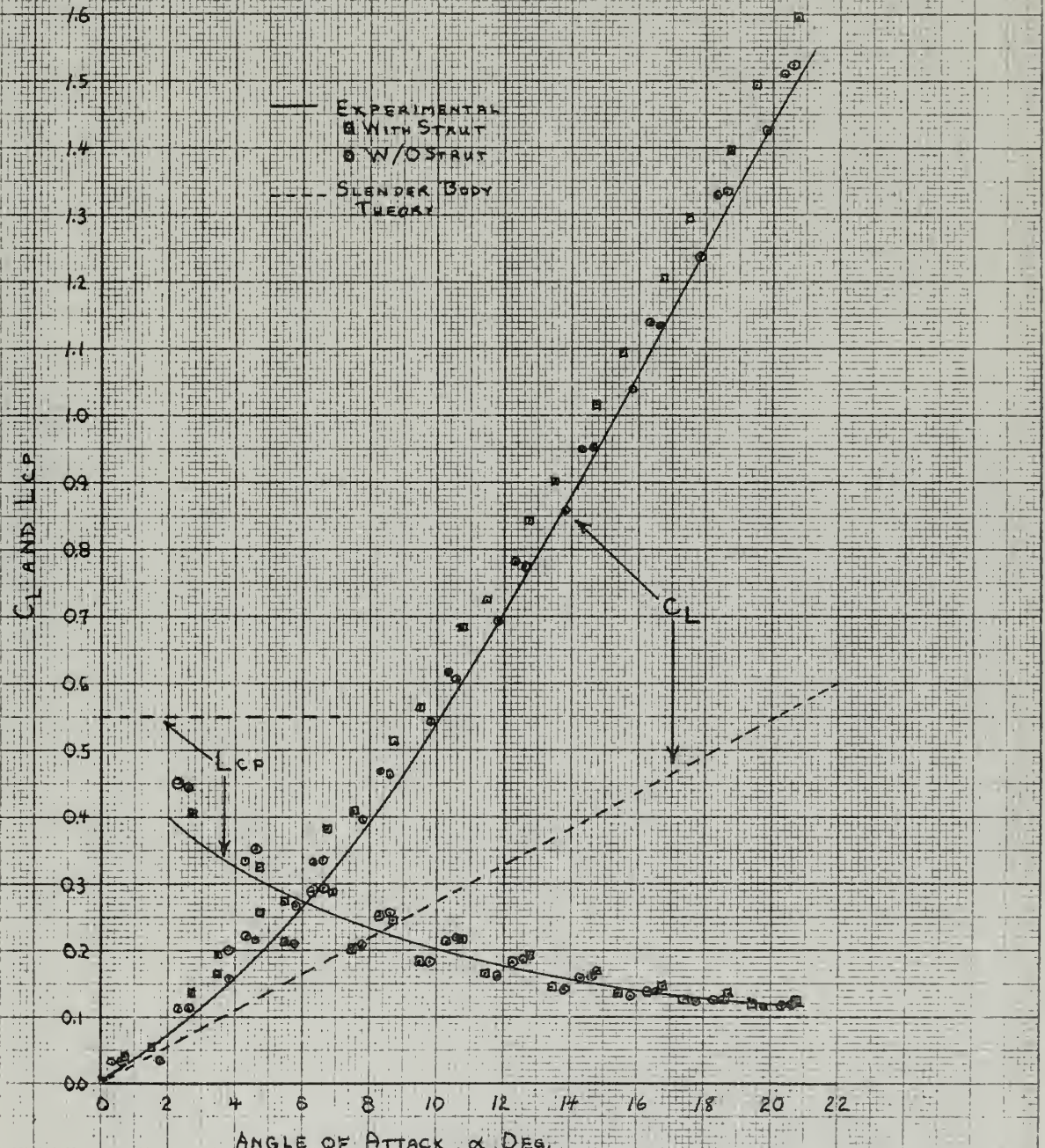

FIGURE 4

FULL FISH

VELOCITY 13 FPS

C_L AND L_{CP}

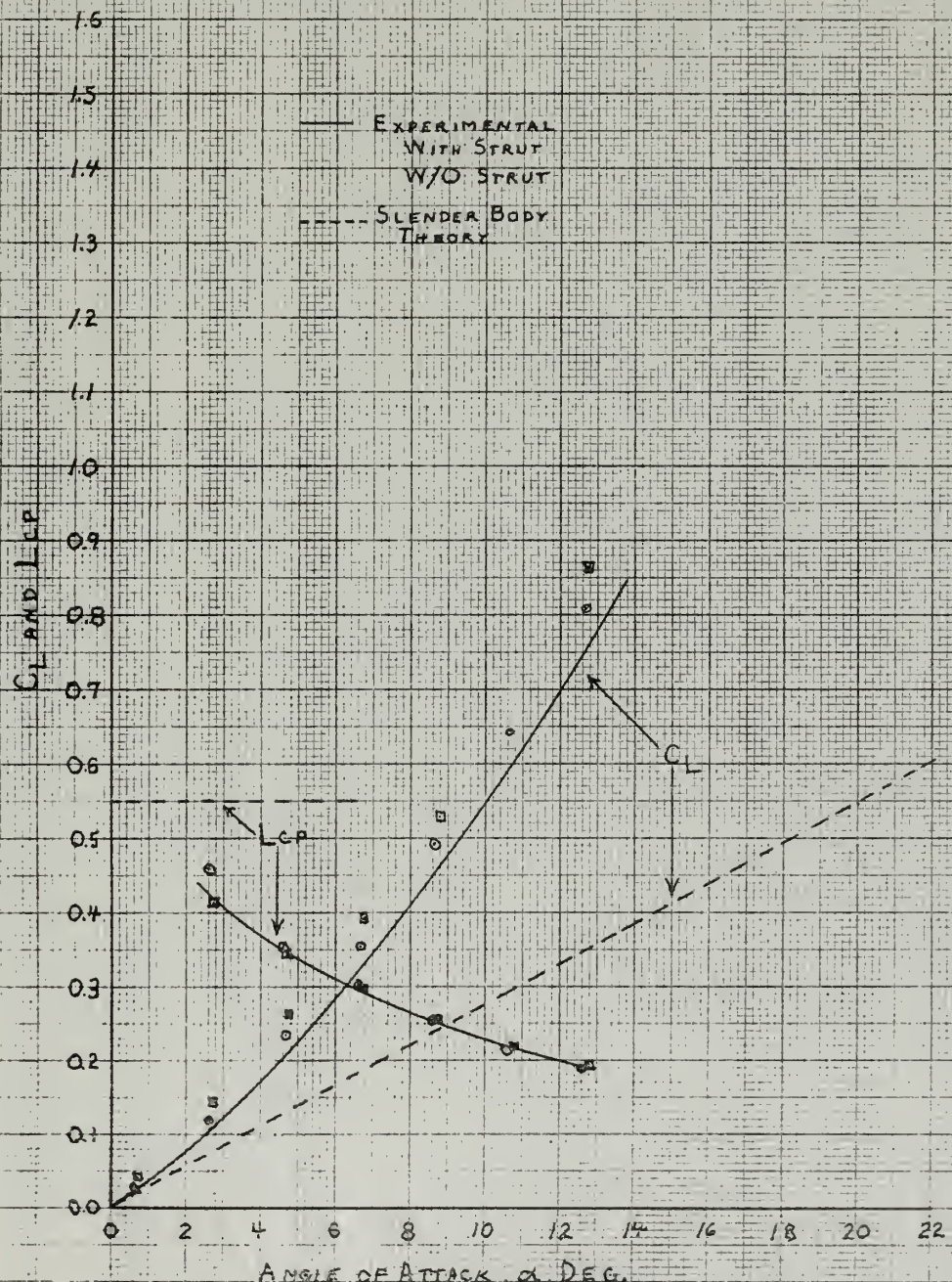

FIGURE 5

FISH BODY

VELOCITY 5 FPS

C_L AND L_{CP}

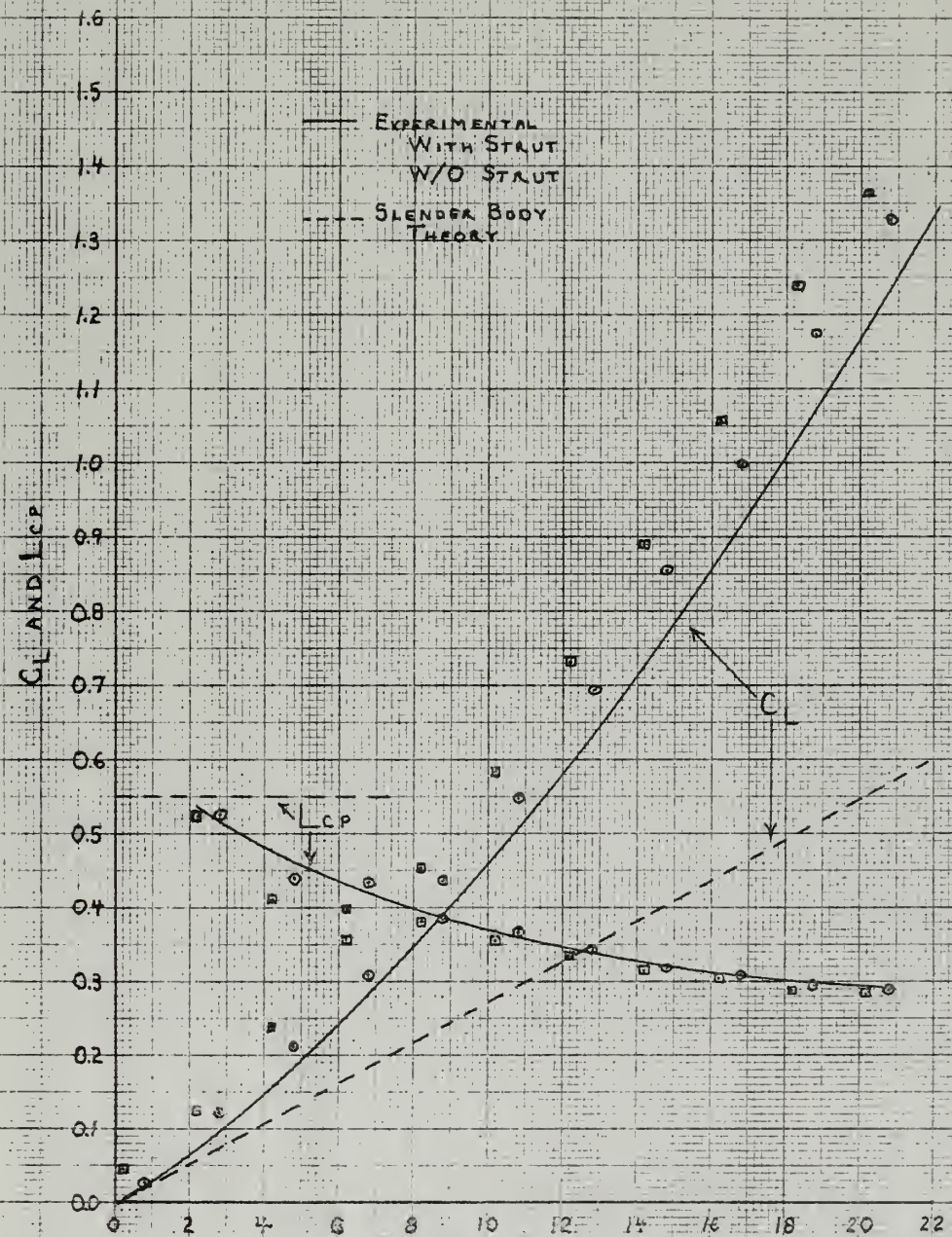

FIGURE 6

FISH BODY

VELOCITY 10 FPS

C_L AND L_{CP}

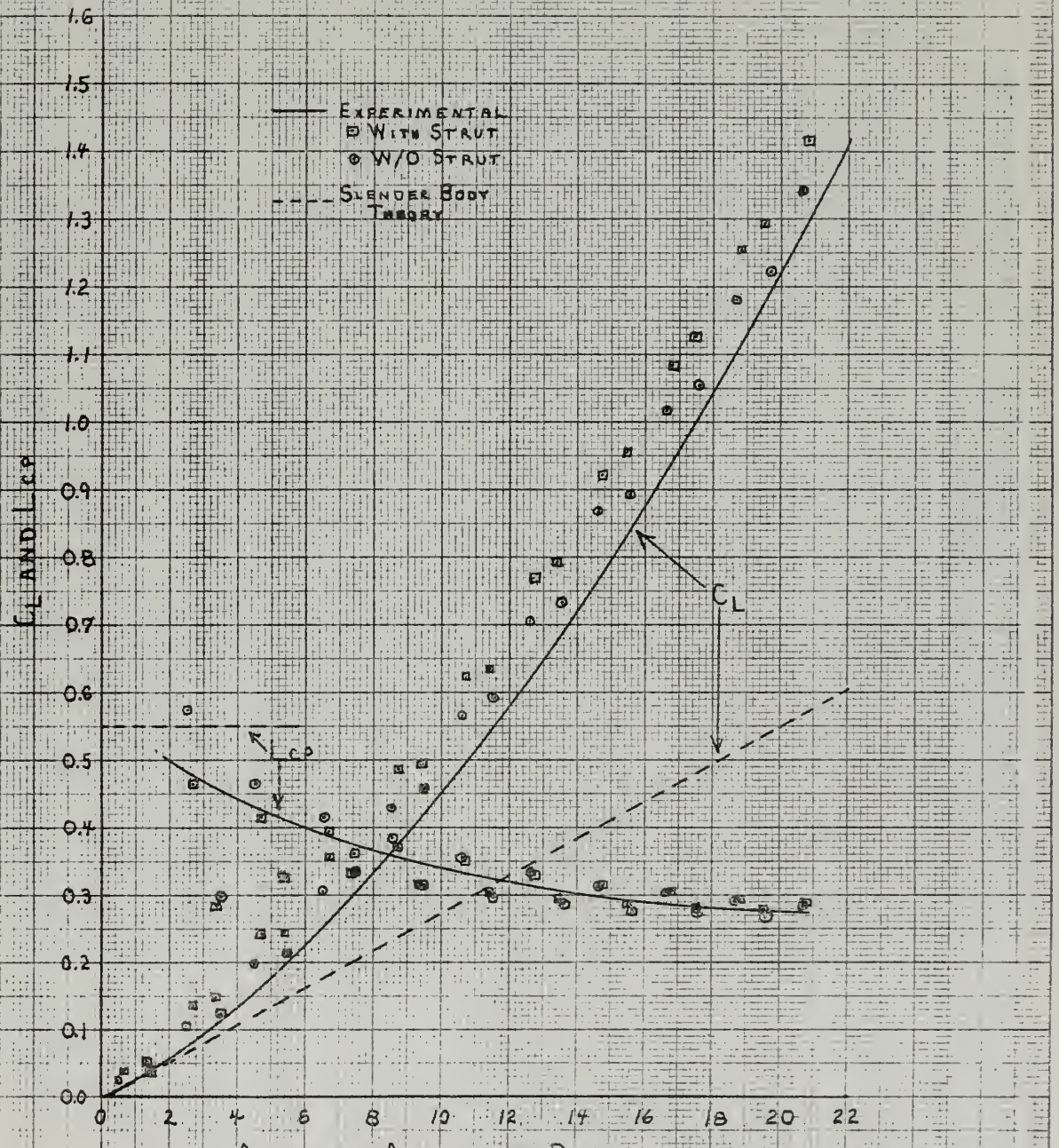

FIGURE 7

FISH BODY

VELOCITY 13 FPS

C_L AND L_{CP}

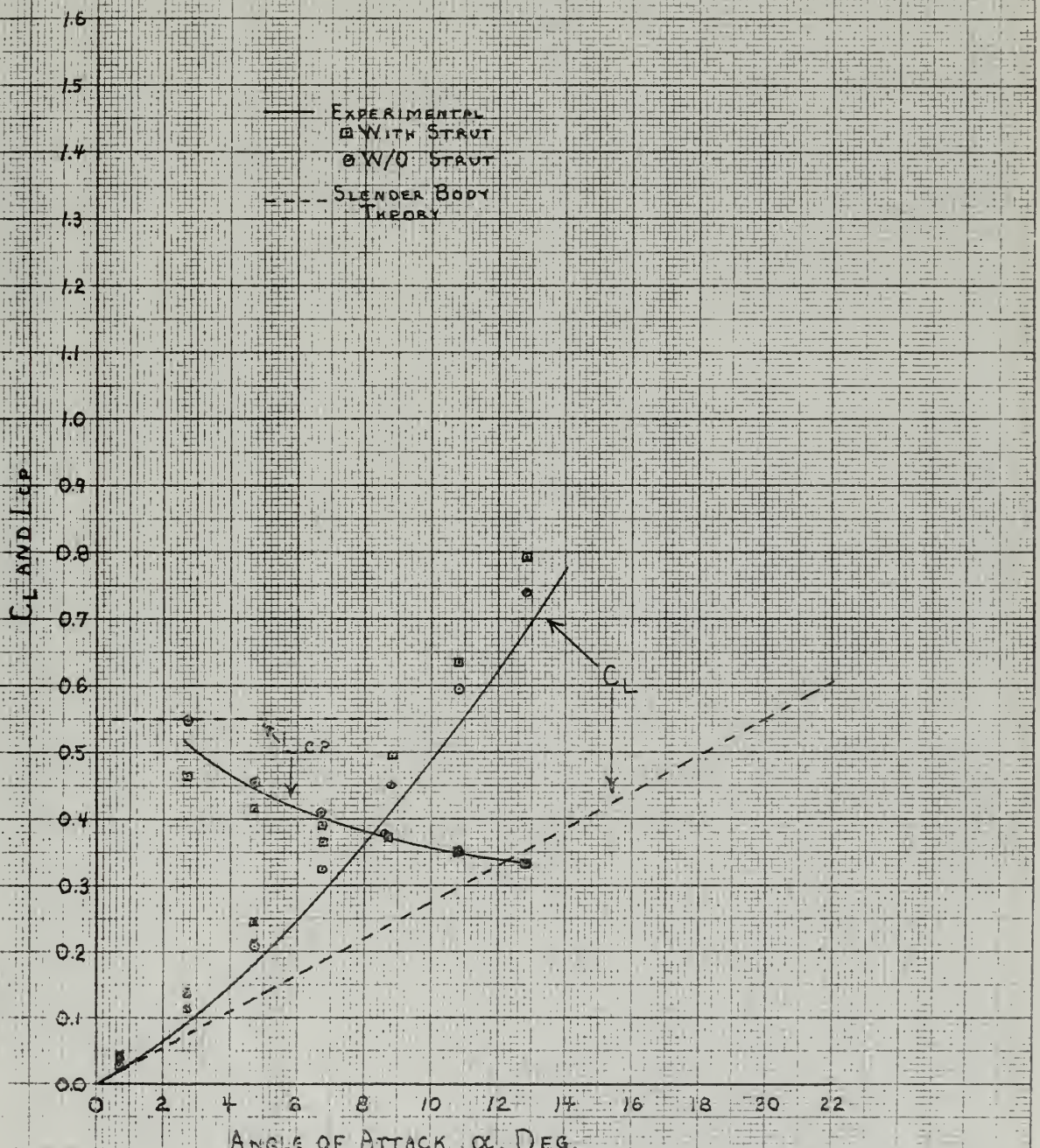

FIGURE 8

FISH HEAD

VELOCITY 5 FPS

C_L AND L_{CP}

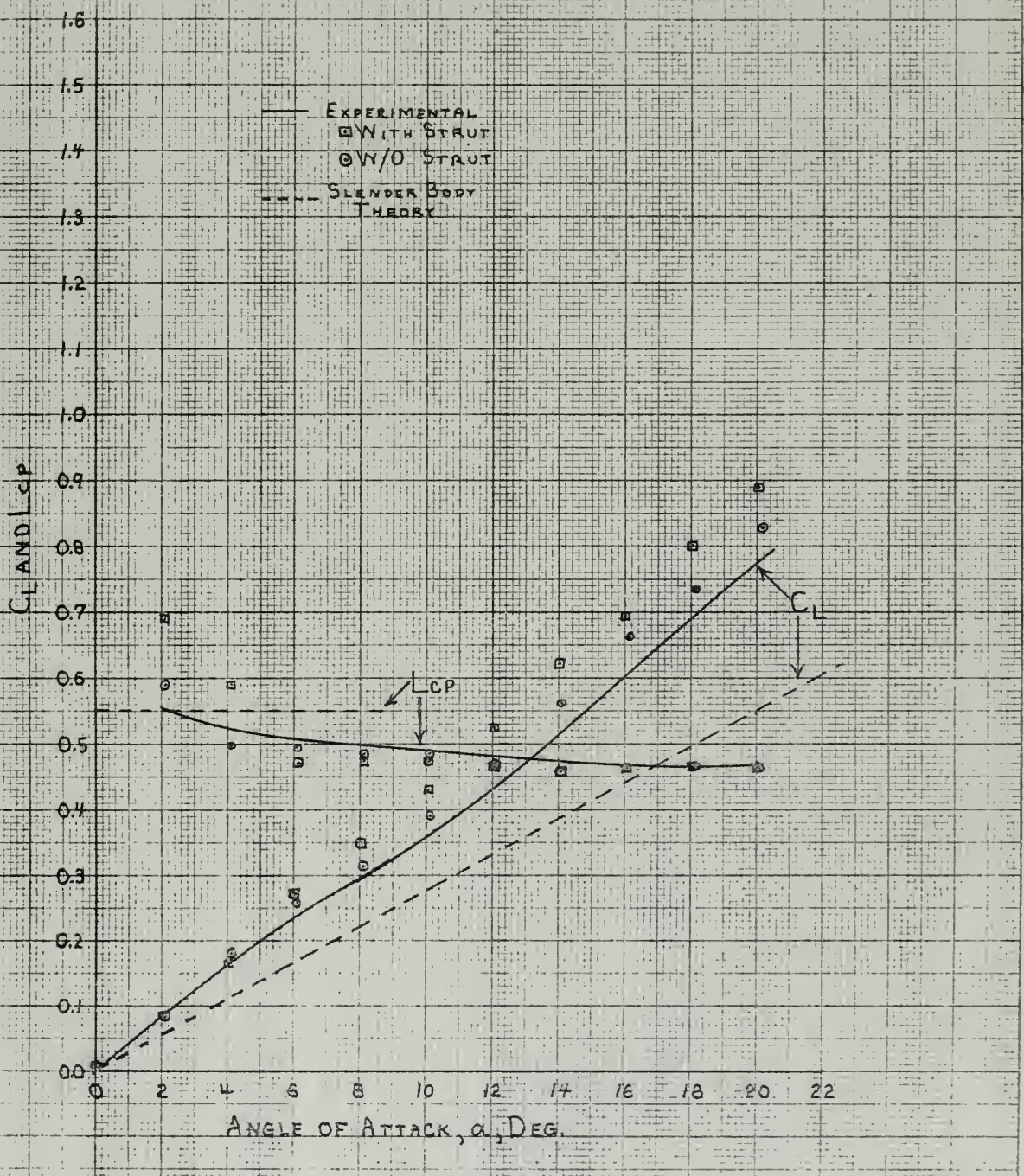

FIGURE 9

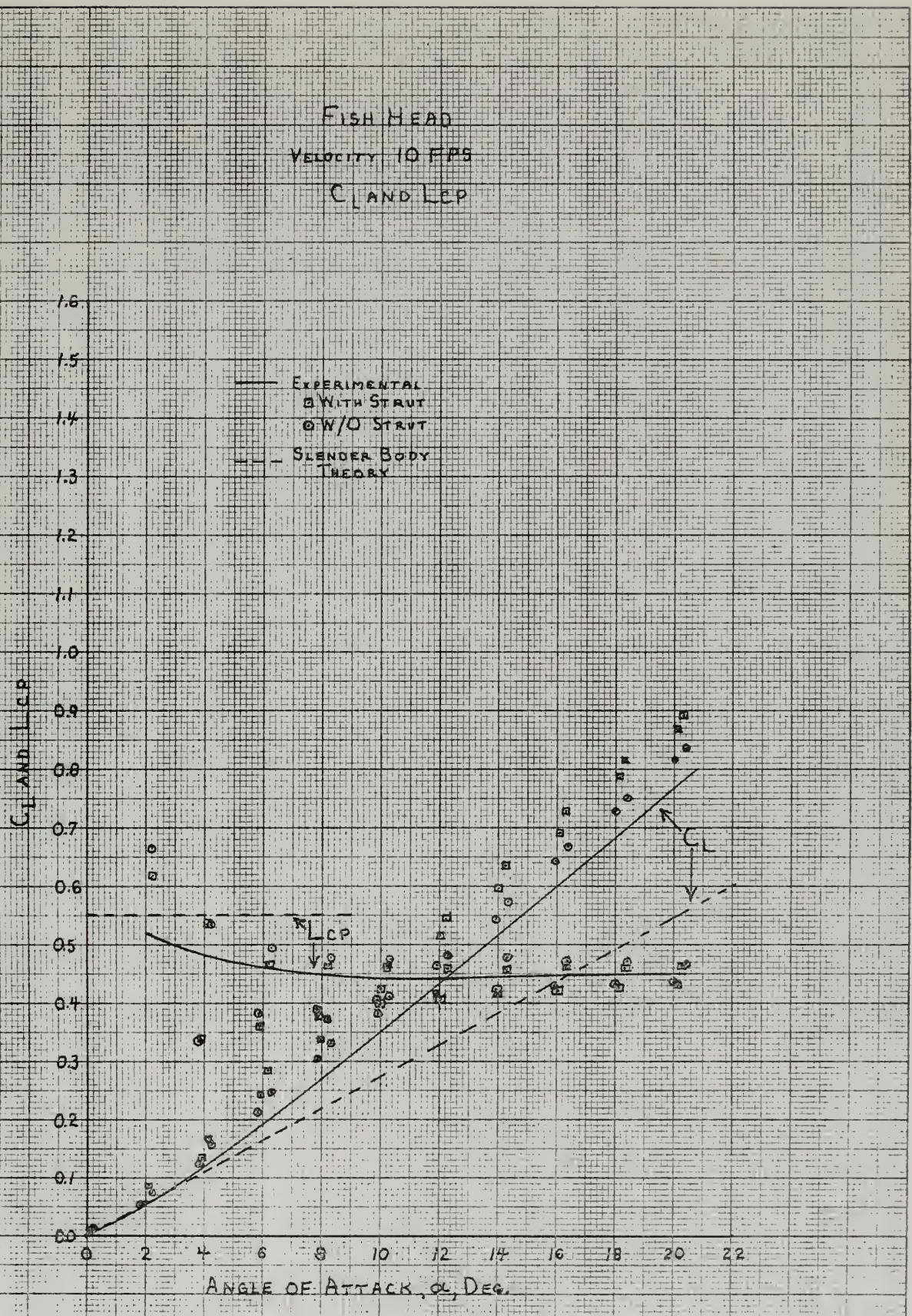
FISH HEAD
VELOCITY 10 FPS
C_L AND L_{CP}
EXPERIMENTAL
WITH STRUT
W/O STRUT
SLENDER BODY THEORY
C_L AND L_{CP}
L_{CP}
C_L
ANGLE OF ATTACK, α, DEG.

FIGURE 10

FISH HEAD

VELOCITY 13 FPS

C_L AND L.C.P

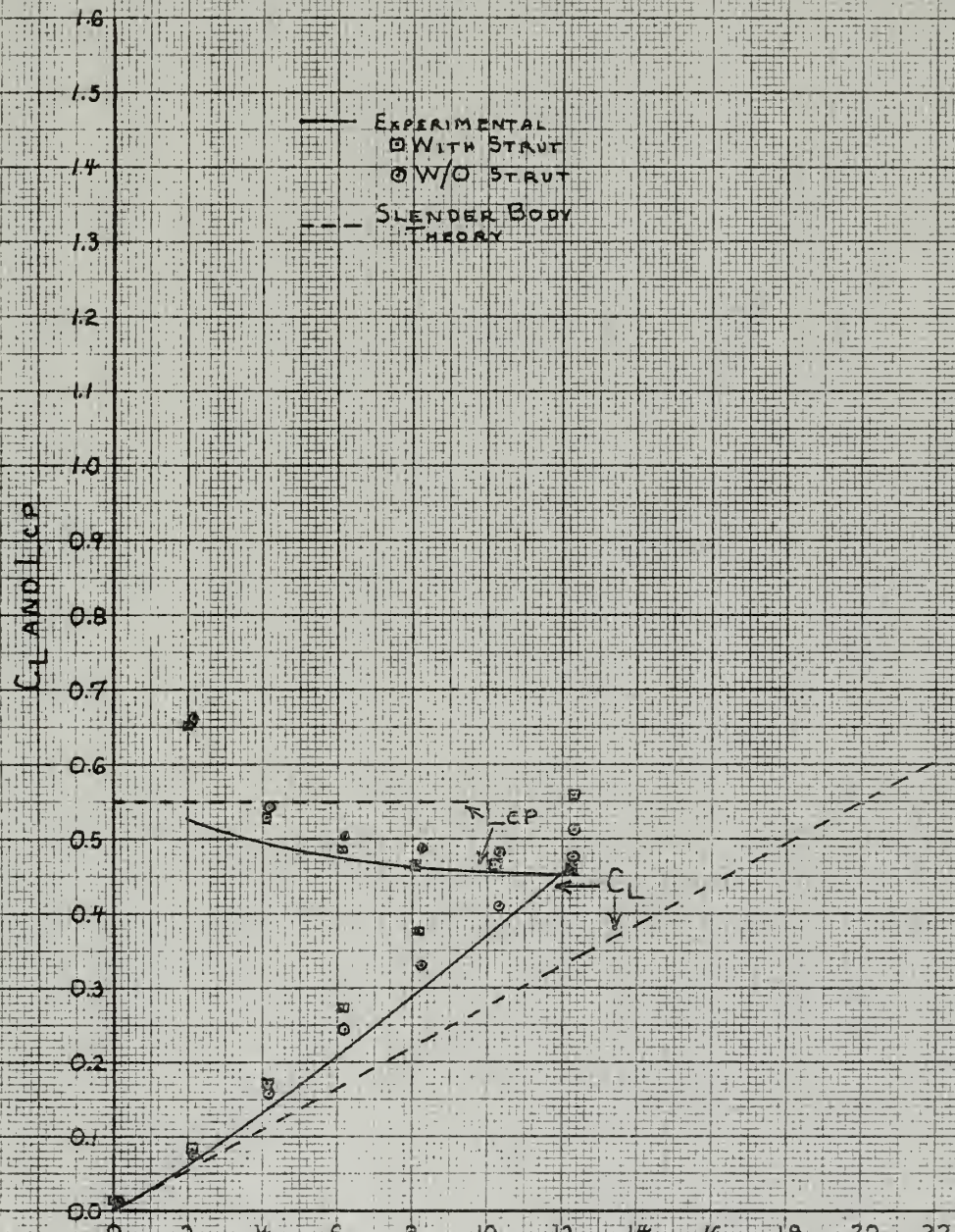

FIGURE 11

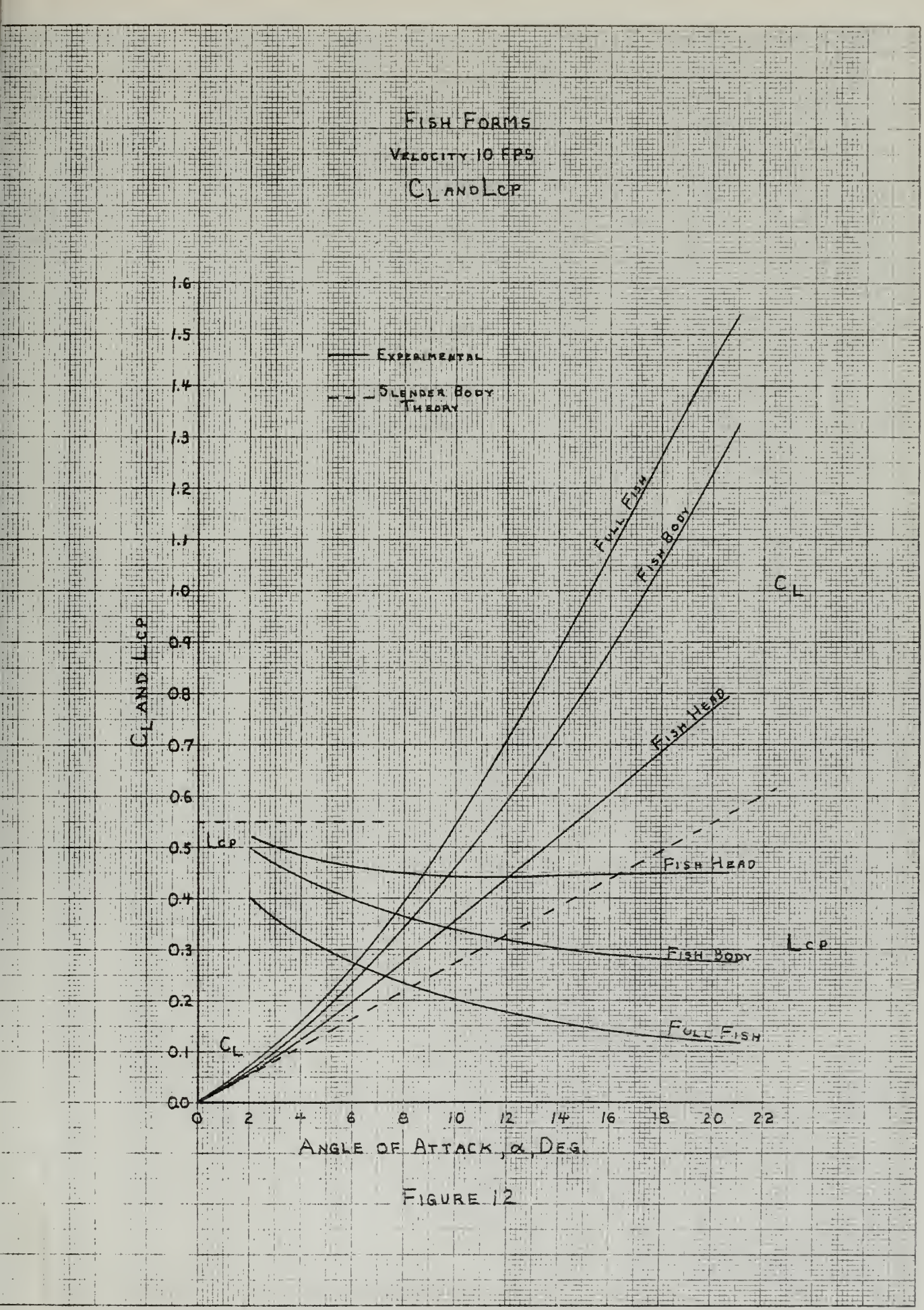
FISH FORMS
VELOCITY 10 FPS
C_L AND L_{CP}
EXPERIMENTAL
SLENDER BODY THEORY
FULL FISH
FISH BODY
FISH HEAD
C_L
L_{CP}
C_L AND L_{CP}
ANGLE OF ATTACK, α, DEG.
1.6
1.5
1.4
1.3
1.2
1.1
1.0
0.9
0.8
0.7
0.6
0.5
0.4
0.3
0.2
0.1
0.0
0
2
4
6
8
10
12
14
16
18
20
22

FIGURE 12

FULL FISH

REDUCED C_L

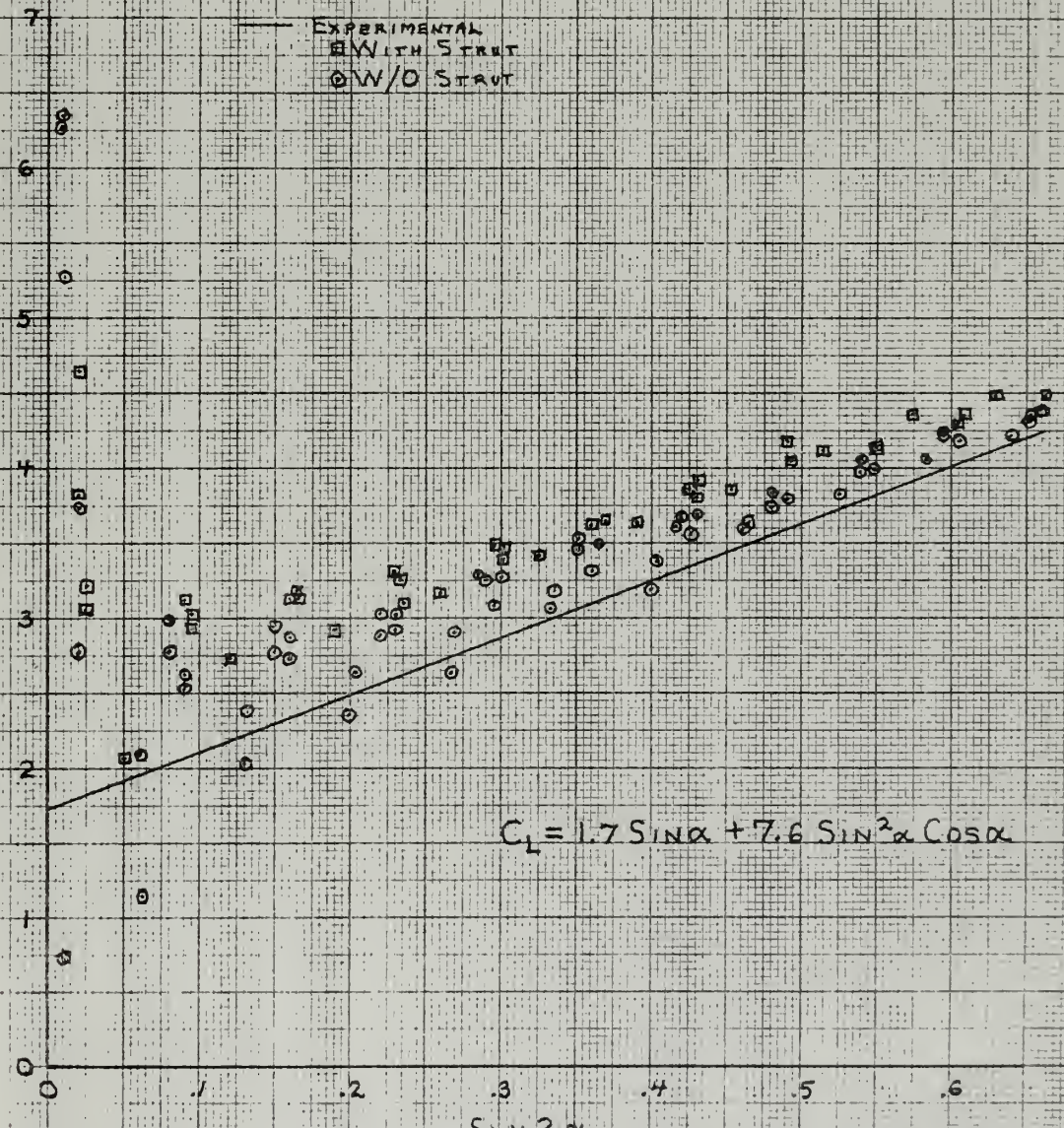

FIGURE 13

FISH BODY

REDUCED C_L

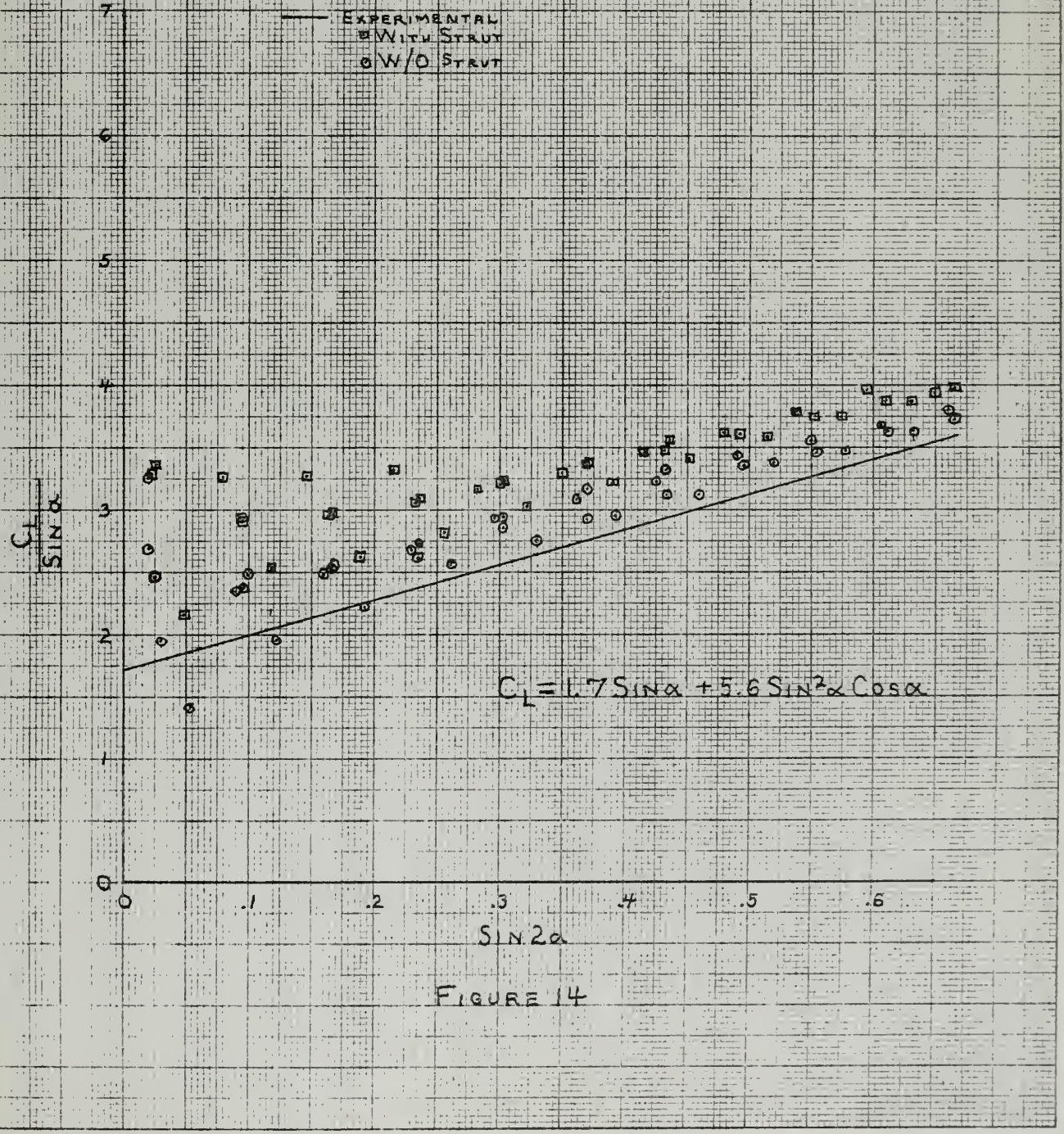

FIGURE 14

FISH HEAD

REDUCED C_L

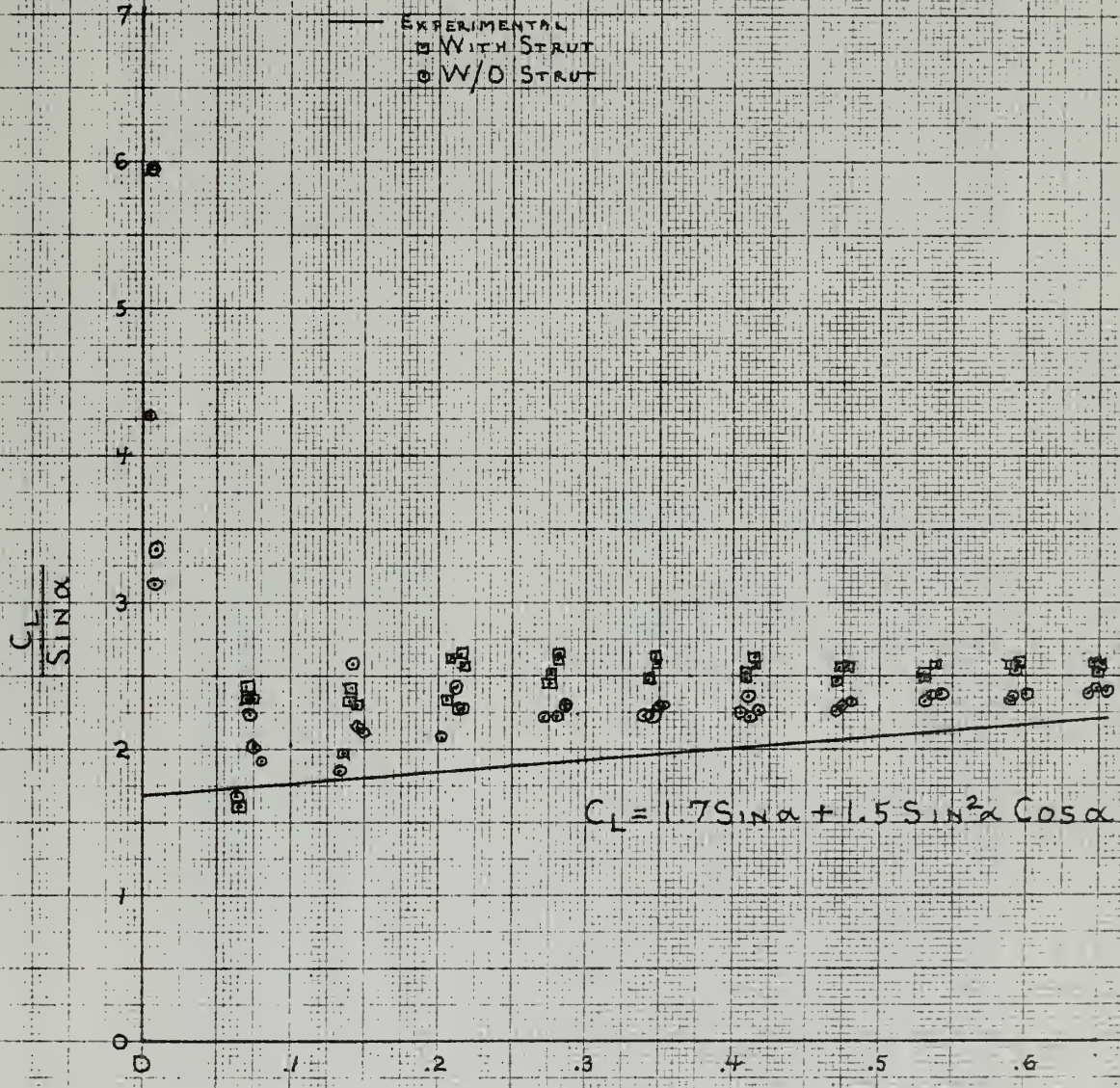

FIGURE 15

Flash Bulb

Figure 16

α = 5.5 deg V = 18.0 fps f = 3.0 cps

Figure 17

α = 7.5 deg V = 18.2 fps p = 3.2 psia

Figure 19

α = 7.5 deg V = 18.1 fps p = 3.2 psia

Figure 20

α = 10.5 deg V = 16.4 fps p = 3.2 psia

Figure 20

α = 10.5 deg V = 16.5 fps p = 3.2 psia

Figure 21

α = 13.5 deg V = 15.9 fps p = 3.7 psia

Figure 22

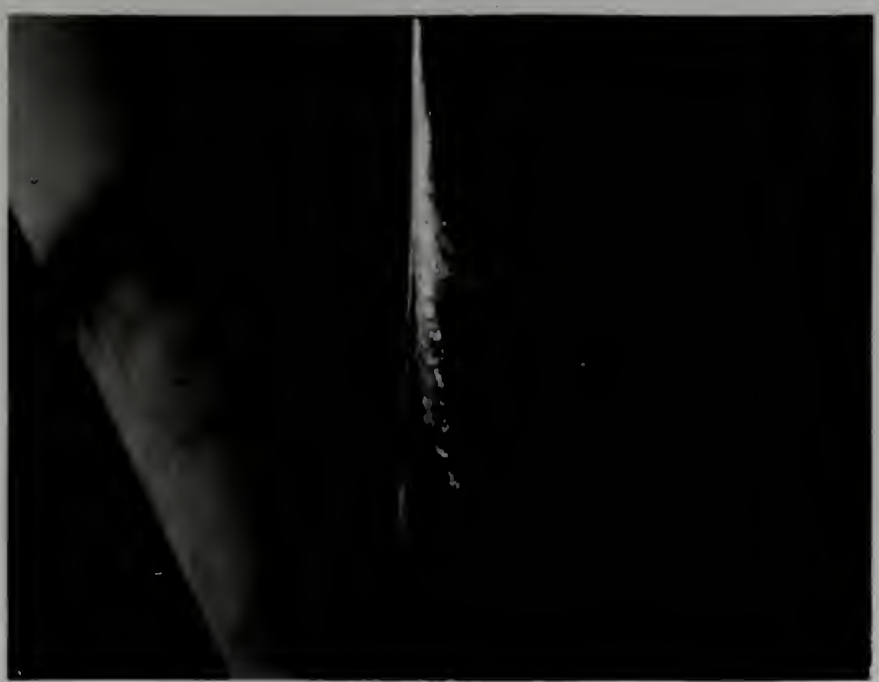

α = 13.5 deg V = 15.7 fps p = 1.2 psia

Figure 23

CHAPTER V - DISCUSSION OF RESULTS

Inspection of the plots of C_L in Figure 12 shows that C_L is a highly non-linear function of angle of attack. It is most non-linear for the full fish and least non-linear for the fish head as would be expected. The Lcp curves show that as the non-linear lift becomes more important, the center of pressure moves aft, being farthest aft for the fish with the tail indicating that the lift contribution of the tail must certainly be a second-order effect. These curves, while giving correct general trends, should be utilized with care as they are merely simple fairings of experimental data approximately corrected for strut interference.

Figures 13, 14 and 15 give expressions for C_L which have been graphically determined from the reduced C_L plots. The linear term in C_L for all three forms has the same value of approximately 1.7. This shows that there is no linear lift contribution from the tail or the body behind the point of maximum span. This value of 1.7 is compared with a value of 1.57 predicted by slender body theory. It is felt that this increase in the linear term is due to the fact that the head of the fish is not "slender", having an aspect ratio of 0.98. This conclusion, however, does not seem to be confirmed by data from other sources so that perhaps there may be some other more subtle effect at work here.

Comparing the lift contribution of the tail and the lift of the head alone (which can be visualized as a tail without a body) shows that at α = ten degrees the lift of the tail behind the body is only 40% of what it would be for the same angle of attack without the body. At 20 degrees the tail contributes about 51% of the lift it would at the same α in free stream.

The non-linear term in C_L is seen to increase as the area is increased by adding a body and then a tail in turn. This non-linear term is not adequately predicted by the mathematical models considered. It is seen, however, that the model using the vortex sheet shed behind the head does predict the right kind of effect, but not in sufficient amount.

CHAPTER VI - CONCLUSIONS AND RECOMMENDATIONS

It is now possible to suggest answers to the three questions posed at the outset. First, it is concluded that for the case investigated, linear slender body theory is inadequate above about two degrees, but fairly accurate at angles of attack of less than two degrees. Further, in answer to the question of linearity, it would appear that the non-linear terms are important for even small angles, thus limiting the value of a strictly linear approach.

With regard to the effect of the body on the tail, it is seen that the body greatly reduced the lift contributed by the tail. The effect varies from completely eliminating the tail lift as the angle of attack goes to zero, to reducing it to about one half of the free stream value at α = 20 degrees.

The experimental results show that the theory developed in this investigation is not adequate. It is felt that a theory which more accurately deals with finite aspect ratio and the non-linear lift associated with vorticies shed from the leading edge is needed. Also a theory to predict the lift on the tail in non-uniform flow is needed.

BIBLIOGRAPHY

1. Lighthill, M. J., "Mathematics and Aeronautics," The Journal of the Royal Aeronautical Society, Vol. 64, July 1960, pp. 375 - 394

2. Lighthill, M. J., "Note on the Swimming of Slender Fish," Journal of Fluid Mechanics, Vol. 9, 1960, pp. 305 - 317

3. Lighthill, M. J., "Hydrodynamics of Aquatic Animal Propulsion," Annual Review of Fluid Mechanics, Vol. 1, 1969, Annual Reviews, Inc., Palo Alto, California, pp. 413 - 445

4. Lighthill, M. J., "Aquatic Animal Propulsion of High Hydromechanical Efficiency," Journal of Fluid Mechanics, Vol. 44, Part 2, 1970, pp. 265 - 301

5. Newman, J. N., Letter of 25 February 1971 (unpublished)

6. Thwaites, Bryan, Incompressible Aerodynamics, Oxford at the Clarendon Press, Oxford, 1960

7. Wu, T. Y., "Effect of Side-Fin Vortex Sheet on Swimming of Slender Fish," Jubilee Memorial W. P. A. van Lammeren 1930 - 1970, Netherlands Ship Model Basin, Wageningen, The Netherlands, 1970

8. Wu, T. Y., "Hydromechanics of Swimming Propulsion, Part III, Swimming and Optimum Movements of Slender Fish with Side Fins," Journal of Fluid Mechanics, Vol. 46, Part 3, 1971, pp. 545 - 568

APPENDIX A

FISH DESIGN

The fish body width was chosen as four inches and the tail width was chosen as three inches in order to keep the fish area small compared to the area of the 20-inch square test section. An overall length of $16\frac{1}{4}$ inches was chosen to make the fish slender and so that the tail would not approach the wall too closely as the fish was given angle of attack.

The lift and moment on the fish was computed using slender body theory.

For head:

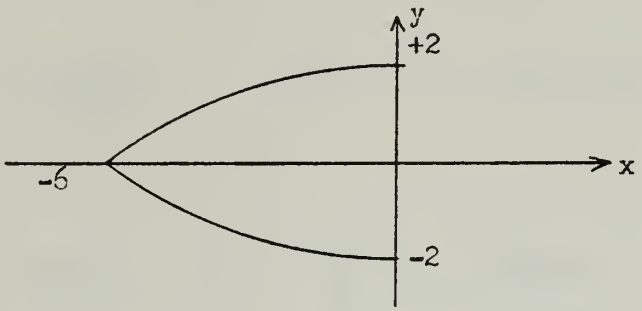

$$y = \pm\, h(x) = \pm \left[(10^2 - x^2)^{\frac{1}{2}} - 8\right]$$

$$L = +\rho U^2 \alpha \pi\, h^2(0)$$

$$L = \rho U^2 \alpha \pi \left(\frac{4 \text{ in.}^2}{144 \text{ in.}^2/\text{ft.}^2}\right)$$

$$M = \int_{-l_{L.E.}}^{0} x l(x)\, dx$$

$$M = \rho U^2 \alpha \pi \int_{-l_{L.E.}}^{0} x \frac{d(h^2)}{dx}\, dx$$

Integrating by parts:

$$M = \rho U^2 \alpha \pi \left[x h^2 \Big|_{-l_{L.E.}}^{0} - \int_{-l_{L.E.}}^{0} h^2 dx \right]$$

$$M = -\rho U^2 \alpha \pi \int_{-l_{L.E.}}^{0} h^2 dx$$

$$M = \frac{-\rho U^2 \alpha \pi}{(12)^3} \int_{-6}^{0} \left[(10^2 - x^2)^{\frac{1}{2}} - 8 \right]^2 dx$$

$$M = \frac{-\rho U^2 \alpha \pi}{(12)^3} \int_{-6}^{0} \left[(10^2 - x^2) - 16 (10^2 - x^2)^{\frac{1}{2}} + 8^2 \right] dx$$

$$M = \frac{-\rho U^2 \alpha \pi}{(12)^3} \left[164x - \frac{x^3}{3} - 8 \left(x \sqrt{10^2 - x^2} + 10^2 \sin^{-1} \left(\frac{x}{a} \right) \right) \right]_{-6}^{0}$$

$$M = \frac{\rho U^2 \alpha \pi}{(12)^3} \left[-984 + 72 - 8 \left(-48 + 100 \sin^{-1} \left(\frac{-6}{10} \right) \right) \right]$$

$$M = \frac{\rho U^2 \alpha \pi}{(12)^3} \left[13.20 \right]$$

$$lcp_{Dim.} = \frac{M}{L} = \frac{\rho U^2 \alpha \pi (12)^2}{\rho U^2 \alpha \pi (12)^3} = \left(\frac{13.20}{4} \right)$$

$$lcp_{Dim.} = \left(\frac{3.30}{12} \right) \text{ ft.} = 3.30 \text{ inches from axis}$$

Reducing these quantities for comparison with the experimental data we define:

$$C_L \equiv \frac{L}{\frac{1}{2}\rho U^2 (2h(0))^2}$$

$$C_L = \frac{\rho U^2 \alpha \pi \ h^2(0)}{\frac{1}{2}\rho U^2 (2h(0))^2}$$

$$C_L = \frac{\pi}{2} \alpha = (1.5708)\alpha$$

$$Lcp \equiv \frac{lcp_{Dim.}}{6 \text{ in.}}$$

$$Lcp = \frac{3.30}{6.00} = 0.55$$

The above analysis was used to estimate the maximum loads and moments likely to be encountered in testing the fish forms. Since it was uncertain as to how much lift the tail surface would contribute, it was assumed that it would lift as though the body was not there in order to obtain a maximum possible lift and moment.

The fish and mounting shaft were fabricated from 2024T3 wrought aluminum alloy with a yield strength of 50,000 psi. The fish was attached to the shaft by clamping a tab from the fish into a slot cut in the shaft. It was originally desired to neck the 3/4 inch shaft to 1/2 inch diameter at the fish, but this resulted in excessive stress. To keep the stress levels low, the full 3/4 inch slotted shaft was carried 5/16 of an inch onto the fish and the tab was given 5/8 inch radius fillets at the fish edge.

A fitting was fabricated and installed in the test section on the side opposite the dynamometer in which the fish was mounted. This fitting allowed a dummy shaft to be placed next to the fish in the same position as the mounting shaft except on the other side of the fish.

APPENDIX B

FORCE DYNAMOMETER

The experimental force measurements were made using the existing rudder force dynamometer. A schematic of the dynamometer is shown in Figure 26. Lebow strain gauge load cells with digital readout boxes were used. The lift load cell was 50-pound maximum load and the moment and drag load cells were ten-pound maximum load. The load cells were mounted between piano wire flexures to make them as soft as possible to lateral deflection. As installed, the flexures absorbed about 11% of the applied drag and moment and about 6% of the lift. This proved to be no problem as the load cells were calibrated in the rig and no significant cross coupling was detected.

The dynamometer is so constructed that the force measuring blocks move with the fish form as the angle of attack is changed. In light of this, the computer program for data reduction performs a coordinate transformation to resolve the forces into streamwise lift and drag forces, as well as converting the digital strain gauge readouts to forces and moments.

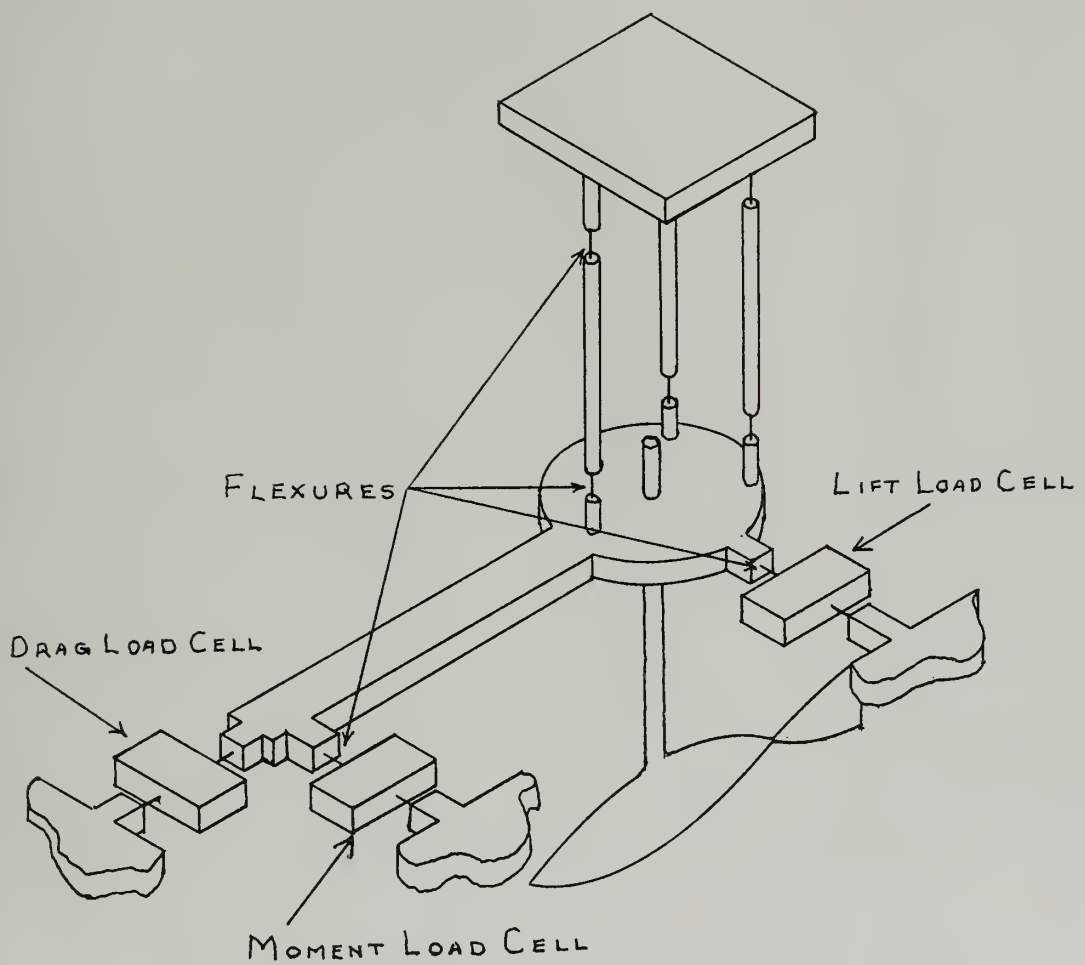

DYNAMOMETER SCHEMATIC

FIGURE 26